



# Investigation on the coupling effect of thermochromism and microstructure on spectral properties of structured surfaces

Junfei Fang, Yimin Xuan\*, Qiang Li, Desong Fan, Jinguo Huang

School of Energy and Power Engineering, Nanjing University of Science & Technology, Nanjing 210094, China

## ARTICLE INFO

### Article history:

Received 5 February 2012

Received in revised form 3 April 2012

Accepted 3 April 2012

Available online 7 April 2012

### Keywords:

Emittance

Thermochromic effect

Structured surface

## ABSTRACT

This paper is aimed at studying the coupling effect of thermochromism and surface microstructure on the spectral properties of structured surfaces. We prepare the samples of structured surfaces of perovskite-type manganese thermochromic materials by patterning one-dimensional gratings and two-dimensional cavity arrays by means of the photolithographic technique. Experiment on radiative properties of these samples indicates that the emittance of the structured surfaces dramatically increases compared with that of the bulk thermochromic materials. It is demonstrated the adjustable emittance range of the thermochromic materials can be effectively enlarged by designing the surface morphology. This implies a novel approach for improving the thermochromic effect of the perovskite-type manganese materials.

© 2012 Elsevier B.V. All rights reserved.

## 1. Introduction

In the past decade or more, plenty of attentions have been attracted on the control of spectral characteristics by using periodic surface structures with the characteristic dimensions on the order of wavelength or sub-wavelength. Tsai et al. [1] designed a type of narrow-band thermal emitter by using the surface plasmon polaritons between Ag thin film with periodic cavity array and Si thin film. Liu et al. [2] obtained a photonic crystal filter by using alternate Si/SiO<sub>2</sub> thin films based on the photonic bandgap effect and applied it to the solar thermophotovoltaic generation systems. Kusunoki et al. [3] and Huang et al. [4] analyzed the enhancement of thermal radiation of tungsten grating surface from the perspective of microcavity effect. Huang et al. [5] proposed a La<sub>0.825</sub>Sr<sub>0.175</sub>MnO<sub>3</sub> structured surface patterned with a series of grating for selective improvement of thermal emission based on the surface topographies and theoretically investigated the microcavity effect. All these examples suggest that it is feasible to control the spectral properties of structured surfaces by designing their appropriate surface topographies.

Recently, the perovskite-type manganese oxides have been extensively studied for their smart thermochromic features, i.e., the spectral properties of these oxides drastically change [6,7] with temperature. Perovskite-type manganese oxide expressed as RMnO<sub>3</sub> is a type of materials with temperature-dependent emittance. Here R stands for trivalent rare earth elements such as La, Pr, Nd, etc. In some cases the perovskite-type oxides may

be R<sub>1-x</sub>A<sub>x</sub>MnO<sub>3</sub> [8–10], in which elements Sr, Ca or other divalent alkaline earth elements can be doped at the A-site. When the doping concentration is proper, the perovskite-type manganese oxide experiences a phase transition from ferromagnetic metallic state to paramagnetic insulating state in the vicinity of Curie temperature  $T_c$ , thus shows unique optical, electrical, and magnetic properties, etc. [10]. Most of such materials exhibit their temperature-dependent spectral characteristics within the temperatures range between 173 K and 373 K. The existing investigation efforts reveal that perovskite-type manganese oxides have higher emittances at higher temperatures and lower emittances at lower temperatures, which corresponds to the metal-insulator transition of the oxides in the vicinity of Curie temperature  $T_c$ . It is well-known now that the perovskite-type manganese oxides can be used as self-regulating thermal management materials for modern spacecraft thermal control [11–14] due to their thermochromic properties. Such an intelligent thermal control material can automatically adjust their radiation characteristics according to the device temperature, and regulate the radiative heat transfer between the device and the ambient environment furthermore to achieve intelligent control of the equipment temperature.

The previous studies were mainly devoted to the inherent properties [7,15–17] to study the radiative characteristics of the thermochromic functional surfaces. For instance, Li et al. [10] investigated the effects of doping alkaline metals on Curie temperature and phase-change temperature, and sintering parameters on radiative properties of the perovskite-type thermochromic materials. Shimakawa et al. [12] discussed the effects of doping ratio of the alkaline metals and thickness of the ceramics on emittance of the perovskite-type thermochromic samples. However, due to the limitations of their inherent properties, the adjustable range

\* Corresponding author. Tel.: +86 025 84315488; fax: +86 025 84315991.  
E-mail address: [ymxuan@mail.njust.edu.cn](mailto:ymxuan@mail.njust.edu.cn) (Y. Xuan).

of emittance of this type of thermochromic material may often not be large enough as expected, which affects possible applications of thermochromic materials in intelligent thermal control. Therefore, exploring some effective approaches to improve the thermochromic effect of the material is of great importance for a series of applications [18,19]. In this paper, we conduct a series of experiment of measuring the spectral properties of structured surfaces made of thermochromic materials and exploring the approach to enhance the thermochromic effect of perovskite-type materials by introducing some microstructures. At first, we prepare the bulk perovskite-type manganese thermochromic materials and the thermochromic samples of structured surfaces with one-dimensional gratings and two-dimensional cavity arrays. Then, a series of experiments are carried out to determine the spectral properties of these samples from temperature 173 K to 373 K.

## 2. Experiment

### 2.1. Preparation of bulk thermochromic materials

The bulk perovskite-type manganese materials  $\text{La}_{0.825}\text{Sr}_{0.175}\text{MnO}_3$ ,  $\text{La}_{0.7}\text{Ca}_{0.2}\text{Sr}_{0.1}\text{MnO}_3$  and  $\text{La}_{0.7}\text{Ca}_{0.15}\text{Sr}_{0.15}\text{MnO}_3$  are prepared by the conventional solid-state reaction method [10,15]. The raw materials used during the solid-state reaction processing are  $\text{La}_2\text{O}_3$ ,  $\text{CaCO}_3$ ,  $\text{SrCO}_3$  and  $\text{MnO}_2$  (99.99% purity). They are all pre-roasted at a high temperature for several hours to remove the impurities and water. Once the powder materials cool down to room temperature, these components are mixed and ground in a ball mill, and then put into the muffle to be calcined at 1473 K for 36 h. The calcined powders are re-ground again once and pressed into pellets with  $\varnothing 40\text{ mm} \times 3\text{ mm}$ . The samples are sintered at 1273 K again for 48 h and then furnace-cooled to room temperature. Finally, they are machined into slices with the size  $\varnothing 25\text{ mm} \times 1\text{ mm}$ . After they are incised into slices, the samples are polished to reduce the surface roughness.

### 2.2. Fabrication of thermochromic materials with periodic structured surfaces

The experimental samples of perovskite-type manganese materials with periodic structured surface are fabricated by means of photolithographic technique [20,21]. This technique is a multi-step pattern transferred process. First, the sample coated with photoresist is irradiated in ultraviolet (UV) light under the protection of a mask. The photoresist exposed to light irradiation will be denatured and dissolved and the pattern of the mask is transferred into photoresist for the first time. Subsequently the sample is eroded by chemical solvents. After the pattern is transferred two times, the microstructure is shifted on the surface of the sample.

### 2.3. Testing and characterization

The XRD patterns of the perovskite-type manganese oxides are collected by using a D8 Super Speed diffractometer (Bruker-Axs company, Germany). The surface roughness of the perovskite-type manganese sample is determined with a CSPM5500 scanning probe microscope (Benyuan-nano company, China). The micrographs of the periodic surface structures of the samples are characterized with an OLS3000 confocal laser scanning microscope (Olympus Corporation, Japan). The reflectance spectra of these perovskite-type manganese samples are measured by using a VERTEX 80V Fourier-transform infrared (FT-IR) spectrometer (Bruker Company, Germany).

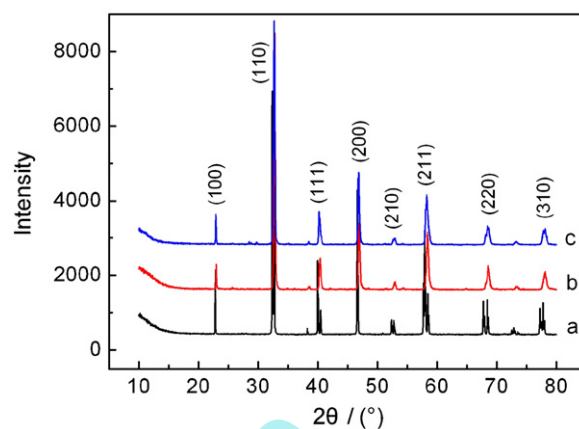


Fig. 1. XRD patterns of the thermochromic materials (a:  $\text{La}_{0.825}\text{Sr}_{0.175}\text{MnO}_3$ ; b:  $\text{La}_{0.7}\text{Ca}_{0.2}\text{Sr}_{0.1}\text{MnO}_3$ ; c:  $\text{La}_{0.7}\text{Ca}_{0.15}\text{Sr}_{0.15}\text{MnO}_3$ ).

## 3. Results and discussion

### 3.1. XRD analysis of the perovskite-type manganese oxides

The corresponding XRD patterns of the perovskite-type manganese materials  $\text{La}_{0.825}\text{Sr}_{0.175}\text{MnO}_3$ ,  $\text{La}_{0.7}\text{Ca}_{0.2}\text{Sr}_{0.1}\text{MnO}_3$  and  $\text{La}_{0.7}\text{Ca}_{0.15}\text{Sr}_{0.15}\text{MnO}_3$  are shown in Fig. 1. These measured curves clearly elucidate that strong diffraction peaks always emerges at the position that  $2\theta$  is equal to  $32^\circ$ , which is the characteristic diffraction peak of the perovskite-type crystal plane (110). The positions of the diffraction peaks are the same as those given in reference [22]. Being contrast to the XRD standard patterns of the perovskite-type materials, we can conclude that all the prepared oxide materials possess the perovskite-type structure. Fig. 1 indicates that the diffraction peaks of patterns b and c shift towards to larger angles of diffraction compared with pattern a. The reason is that due to the introduction of  $\text{Ca}^{2+}$  ion, the interplanar crystal spacing of samples  $\text{La}_{0.7}\text{Ca}_{0.2}\text{Sr}_{0.1}\text{MnO}_3$  and  $\text{La}_{0.7}\text{Ca}_{0.15}\text{Sr}_{0.15}\text{MnO}_3$  becomes smaller than that of sample  $\text{La}_{0.825}\text{Sr}_{0.175}\text{MnO}_3$ . According to Bragg equation, the diffraction peaks will deflect to the larger angle of diffraction [7,23].

### 3.2. Microstructure feature of the structured surfaces

Fig. 2 exhibits AFM image of surface microstructure of the perovskite-type manganese sample after polishing. Evidently, the sample surface is very smooth and the surface roughness is only

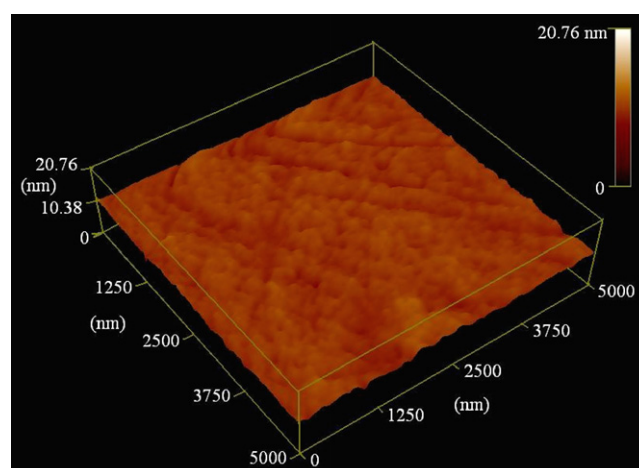
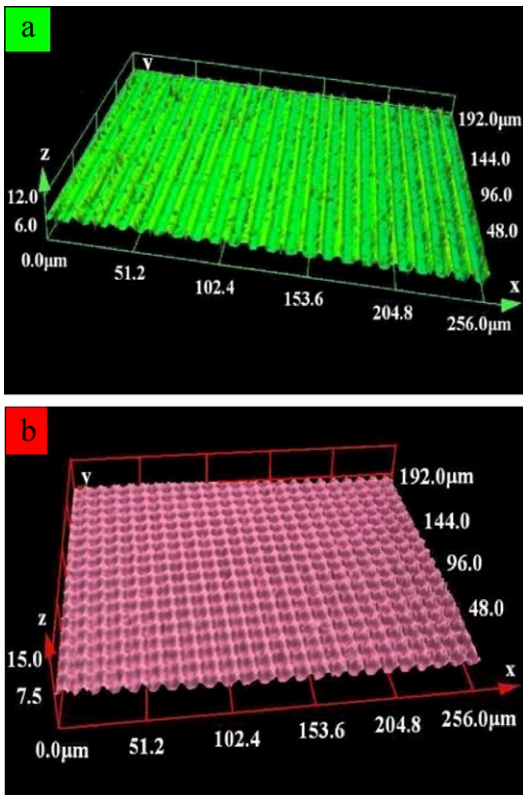


Fig. 2. AFM image of the perovskite-type manganese material.



**Fig. 3.** Micrographs of the perovskite-type manganese materials with periodic structured surface (a: periodic grating structure; b: periodic cavity structure).

several nanometers. Thus, the surface can be considered as optical smooth due to the fact that the roughness is much smaller than the characteristic wavelength corresponding to the experimental temperature range. The micrographs of the periodic surface structures of the samples are shown in Fig. 3. Obviously, the periodic structures are very uniform. Fig. 3(a) shows the image of the structured surface of periodic gratings with the following structural parameters: the period  $10 \mu\text{m}$ , the width of the grating groove  $6.0 \mu\text{m}$ , and the depth  $2.0 \mu\text{m}$ . Fig. 3(b) illustrates the image of the structured surface with periodic cavity arrays with the structural parameters: the period  $10 \mu\text{m}$ , the diameter of the cavity  $6.0 \mu\text{m}$ , and the depth  $2.0 \mu\text{m}$ .

### 3.3. Spectrum and emittance analysis of the thermochromic materials

The measurements of the reflectance spectra ( $R$ ) of these samples within the temperature range from  $173 \text{ K}$  to  $373 \text{ K}$  are carried out by using IR light with a wavelength from  $1.25$  to  $25.5 \mu\text{m}$  with near normal incidence. Fig. 4 gives the IR reflectance spectra ( $R$ ) of the  $\text{La}_{0.7}\text{Ca}_{0.2}\text{Sr}_{0.1}\text{MnO}_3$  material with three different structural surfaces. Fig. 4a–c, respectively, corresponds to the reflectance spectra of the samples without any periodic structure, with periodic grating structure, and with periodic cavity structure. It is clear from the figure that all the reflectance decreases as the temperature rises from  $173 \text{ K}$  to  $373 \text{ K}$ . The reflectance of the samples with both periodic gratings and cavity structures is lower than that of the bulk sample at the same temperature. Especially, this feature becomes more remarkable with shorter wave bands. In fact, the electromagnetic wave entering the grooves of gratings or cavity structure couples with that reflected by walls and undersides of grooves and the standing wave is generated. This phenomenon is so-called the microcavity effect [3,24,25]. The electromagnetic wave is confined

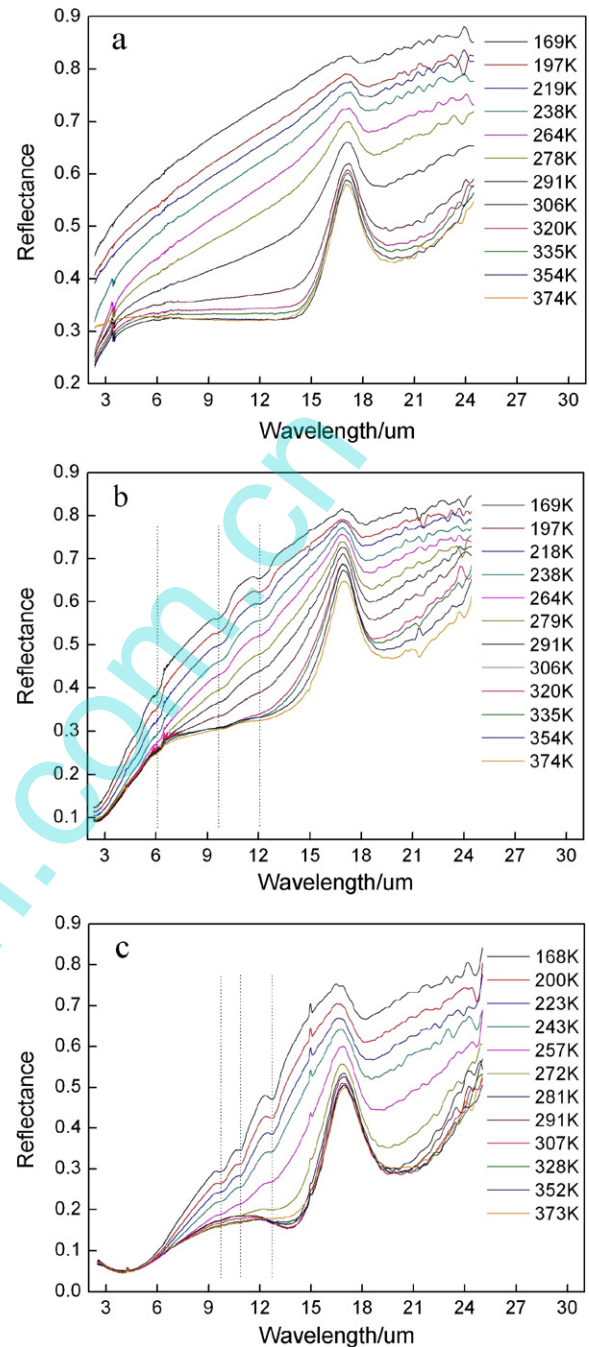


**Fig. 4.** IR reflectance spectra of the  $\text{La}_{0.7}\text{Ca}_{0.2}\text{Sr}_{0.1}\text{MnO}_3$  material with different structural surfaces at different temperatures (a: without periodic structure; b: with periodic grating structure; c: with periodic cavity structure).

in the microstructure when the microcavity effect is excited. Consequently, a reflection dip (i.e., an absorption peak) emerges. It can be found that there are a series of reflection dips in Fig. 4(b) and (c) compared with the curves in Fig. 4(a). In Fig. 4(b), these dips are located at  $12.0 \mu\text{m}$ ,  $9.7 \mu\text{m}$  and  $6.0 \mu\text{m}$ , while these dips are situated at  $12.8 \mu\text{m}$ ,  $10.7 \mu\text{m}$  and  $9.8 \mu\text{m}$  in Fig. 4(c), respectively. For a structured surface of rectangular gratings, there is the relationship between the microcavity resonant wavelength and the structural sizes [26]:

$$\lambda_{mn} \propto \left( \frac{m}{l_g} + \frac{n}{h} \right)^{-1/2} \quad (1)$$

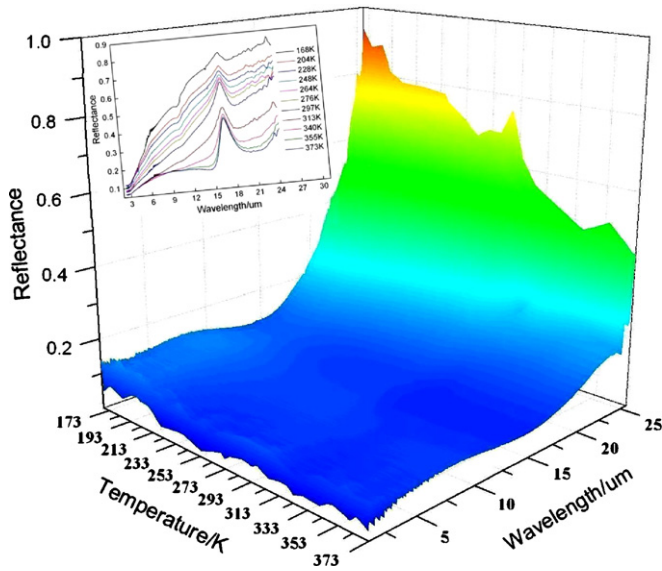


**Fig. 5.** Temperature and wavelength dependences of the reflectance of  $\text{La}_{0.825}\text{Sr}_{0.175}\text{MnO}_3$  with grating structured surface (inset is IR reflectance spectra of the corresponding material at different temperatures, respectively).

where  $l_g$  and  $h$  denote the groove width and depth of the grating, respectively.  $m$  and  $n$  are integers.

Similarly, for a structured surface with cylindrical cavities, the relationship between the microcavity resonant wavelength and the structural sizes can be described as [26]:

$$\lambda_{mn} \propto \left[ \left( \frac{\mu_{mn}}{2\pi R} \right)^2 + \left( \frac{p}{2l} \right)^2 \right]^{-1/2} \quad (2)$$

where  $R$  and  $l$  denote the groove radius and depth of the cavity, respectively.  $\mu_{mn}$  is the  $m$ th root of the  $n$ th order Bessel function and  $p$  is an integer.

According to Eq. (1), the wavelengths resulting from the microcavity resonance are located at  $12.0 \mu\text{m}$ ,  $8.5 \mu\text{m}$  and  $6.9 \mu\text{m}$  for gratings when  $(m, n) = (1, 0)$ ,  $(2, 0)$  and  $(0, 1)$ , respectively. From Eq. (2), one can obtain that the resonant wavelengths are respectively located at  $12.8 \mu\text{m}$ ,  $9.8 \mu\text{m}$ , and  $7.7 \mu\text{m}$  for the cavity arrays when  $(m, n, p) = (1, 1, 0)$ ,  $(1, 0, 0)$  and  $(1, 2, 0)$ . It should be emphasized that both Eqs. (1) and (2) are valid for noble metals. Since the thermochromic material is not an ideal conductor, the data obtained from these formulas are all less than those experimentally observed. The oddish point that the position  $6.9 \mu\text{m}$  obtained from Eq. (1) is greater than the experimentally observed value of  $6.0 \mu\text{m}$  may result from some measured errors for the gratings structure. Therefore, it can be concluded that the reflection dips in Fig. 4(b) and (c) are resulted from the microcavity effect.

Fig. 5 illustrates the temperature and wavelength dependences of reflectance of the grating structured surface of  $\text{La}_{0.825}\text{Sr}_{0.175}\text{MnO}_3$ . The inset is IR reflectance spectra of the corresponding material at different temperatures, respectively. It illustrates a metallic behavior which is indicated by the relatively high reflectance spectra at low temperatures and a nonmetallic feature indicated by the relatively low reflectance spectra at high temperatures. The reflectance decreases markedly with decrease in temperature within the range between 273 K and 313 K. The mutation is due to metal-insulator phase transition, and the Curie temperature  $T_c$  of  $\text{La}_{0.825}\text{Sr}_{0.175}\text{MnO}_3$  prepared here is about 290 K. Also, there is a mutation in the spectra between the temperatures from 264 K to 291 K in Fig. 4(a), which implies that the Curie temperature  $T_c$  of the corresponding sample is about 275 K.

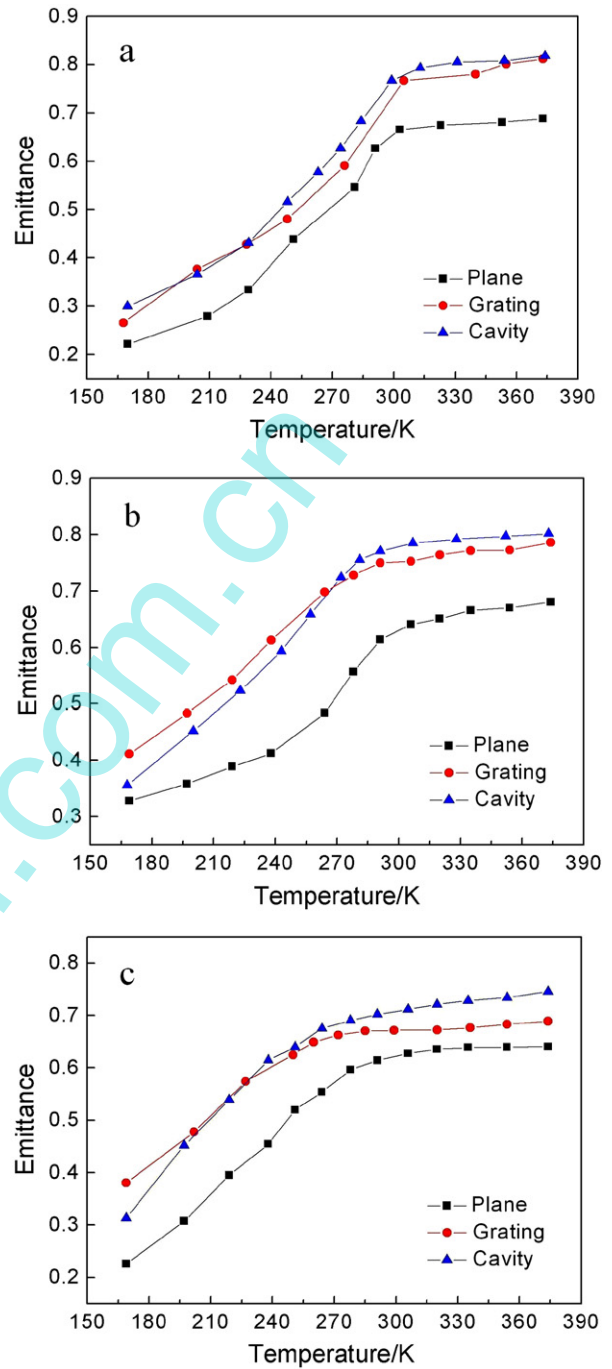


**Fig. 6.** Emittance variation of surfaces of thermochromic materials with temperatures (a:  $\text{La}_{0.825}\text{Sr}_{0.175}\text{MnO}_3$ ; b:  $\text{La}_{0.7}\text{Ca}_{0.2}\text{Sr}_{0.1}\text{MnO}_3$ ; c:  $\text{La}_{0.7}\text{Ca}_{0.15}\text{Sr}_{0.15}\text{MnO}_3$ ; square symbol: without periodic surface structure; circle symbol: with periodic grating structure; triangular symbol: with periodic cavity structure).

The emittance ( $\varepsilon$ ) of the sample at temperature  $T$  can be evaluated from an IR reflectance spectrum ( $R$ ). It is well-known that emissivity of a nontransparent material yields:

$$\varepsilon(\lambda) \equiv 1 - R(\lambda) \quad (3)$$

Thus, the emittance is calculated from the following equation [13]:

$$\varepsilon = \frac{\int [1 - R(\lambda)] I_b(\lambda, T) d\lambda}{\int I_b(\lambda, T) d\lambda} \quad (4)$$

where  $I_b(\lambda, T)$  is the spectral radiance emitted by a blackbody surface.

Fig. 6 exhibits the emittance of the thermochromic materials  $\text{La}_{0.825}\text{Sr}_{0.175}\text{MnO}_3$ ,  $\text{La}_{0.7}\text{Ca}_{0.2}\text{Sr}_{0.1}\text{MnO}_3$  and  $\text{La}_{0.7}\text{Ca}_{0.15}\text{Sr}_{0.15}\text{MnO}_3$  with and without periodic structured surfaces within the temperatures range from 173 K to 373 K. The line with the square symbol is the experimental data for the surface without periodic structures; the line with the circle symbol corresponds to the structured surface with periodic gratings; and the line with the triangular symbol stands for the structured surface with cavity arrays.

As shown in Fig. 6, all the samples have lower emittance at lower temperatures and higher emittance at higher temperatures and exhibit a metal-insulator transition while the temperature rises from 173 K to 373 K. The emittance of the samples increases with increase in temperature, which accords with the spectral properties of this type of thermochromic material. Moreover, the emittance of the samples with the periodic structure remarkably increases compared with the bulk one. Fig. 6(a) indicates that as the temperature increases from 173 K to 373 K, the adjustable ranges of the emittances of the structured surfaces made of  $\text{La}_{0.825}\text{Sr}_{0.175}\text{MnO}_3$  material with gratings and cavity arrays are enlarged to 0.546 and 0.518, respectively, while that of the smooth surface is 0.466, which reveals that the microstructure improves the thermochromic effect of the material. According to the foregoing analysis of performance of the reflectance spectra, we believe that the improvement of thermochromic effect of the sample is resulted from the microcavity effect. And the experimental data coincide very well with the theoretical calculation in Ref. [5]. From the curves shown in Fig. 6(b) and (c), one learns that as the temperature increase from 173 K to 373 K, the adjustable ranges of the emittance of the structured samples made of  $\text{La}_{0.7}\text{Ca}_{0.2}\text{Sr}_{0.1}\text{MnO}_3$  material with gratings and cavity arrays are respectively enlarged to 0.375 and 0.445, while that of the smooth surface of the same material is 0.352. The adjustable ranges of the emittance of the structured surfaces of  $\text{La}_{0.7}\text{Ca}_{0.15}\text{Sr}_{0.15}\text{MnO}_3$  with corresponding structures are about 0.308 and 0.432, while that of the smooth surface is about 0.415. Since the optimized dimension parameters are selected based on the sample  $\text{La}_{0.825}\text{Sr}_{0.175}\text{MnO}_3$ , the adjustable ranges of the structured surfaces of  $\text{La}_{0.825}\text{Sr}_{0.175}\text{MnO}_3$  can be effectively enhanced. These optimized values of components may vary from one perovskite-type oxide to another. Therefore, the optimized component values of  $\text{La}_x\text{Sr}_{1-x}\text{MnO}_3$  may not be suitable for the other samples such as  $\text{La}_{0.7}\text{Ca}_{0.15}\text{Sr}_{0.15}\text{MnO}_3$ . Consequently, with respect to variations of the components, the structural parameters of the structured surfaces need to be appropriately selected so as to effectively regulate the thermochromic effect.

#### 4. Conclusions

In summary, the coupling effects of the thermochromism and microstructure of the perovskite-type manganese thermochromic materials on the spectral properties of structured surfaces have been experimentally studied. The samples of structured surfaces of  $\text{La}_{0.825}\text{Sr}_{0.175}\text{MnO}_3$ ,  $\text{La}_{0.7}\text{Ca}_{0.2}\text{Sr}_{0.1}\text{MnO}_3$  and  $\text{La}_{0.7}\text{Ca}_{0.15}\text{Sr}_{0.15}\text{MnO}_3$  with one-dimensional gratings and two-dimensional cavity arrays have been fabricated by using photolithographic technique. The IR reflectance spectra of these samples with and without periodic structures within the temperatures range from 173 K to 373 K have been obtained by using an FT-IR spectrometer. Experimental results have shown that the emittance of the structured surfaces with periodic structures drastically increases compared with that of the bulk ones. Moreover, the thermochromic effect of  $\text{La}_{0.825}\text{Sr}_{0.175}\text{MnO}_3$  material is remarkably enhanced with both the periodic structures of gratings and cavity arrays, but that of the structured surfaces of  $\text{La}_{0.7}\text{Ca}_{0.2}\text{Sr}_{0.1}\text{MnO}_3$  and  $\text{La}_{0.7}\text{Ca}_{0.15}\text{Sr}_{0.15}\text{MnO}_3$  is enhanced only for the case of cavity arrays. The optimized structural parameters

for enhancing the adjustable capability of the thermochromic effect vary from one type of perovskite-type oxide to another. This indicates that it is feasible to regulate the radiative properties of thermochromic materials by designing their appropriate surface topographies. This work provides some instructive information for the improvement of performance of thermochromic materials.

#### Acknowledgment

This work was supported by the National Natural Science Foundation of China (Grant No. 50936002).

#### References

- [1] M.W. Tsai, T.H. Chuang, C.Y. Meng, Y.T. Chang, S.C. Lee, High performance mid-infrared narrow-band plasmonic thermal emitter, *Applied Physics Letters* 89 (2006) 173116.
- [2] G.P. Liu, Y.M. Xuan, Y.G. Han, Q. Li, Investigation of one-dimensional Si/SiO<sub>2</sub> photonic crystals for thermophotovoltaic filter, *Science China Technological Sciences* 39 (2009) 129–134.
- [3] F. Kusunoki, T. Kohama, T. Hiroshima, S. Fukumoto, J. Takahara, T. Kobayashi, Narrow-band thermal radiation with low directivity by resonant modes inside tungsten microcavities, *Japanese Journal of Applied Physics* 43 (2004) 5253–5258.
- [4] J.G. Huang, Y.M. Xuan, Q. Li, Narrow-band spectral features of structured silver surface with rectangular resonant cavities, *Journal of Quantitative Spectroscopy and Radiative Transfer* 112 (2011) 839–846.
- [5] J.G. Huang, Y.M. Xuan, Q. Li, Investigation on emissive properties of perovskite-type oxide LSMO with grating surface, *Science China Technological Sciences* 54 (2011) 220–225.
- [6] K. Shimazaki, A. Ohnishi, Y. Nagasaka, Development of spectral selective multi-layer film for a variable emittance device and its radiation, *International Journal of Thermophysics* 24 (2003) 757–769.
- [7] G.C. Tang, Y. Yu, Y.Z. Cao, W. Chen, The thermochromic properties of  $\text{La}_{1-x}\text{Sr}_x\text{MnO}_3$  compounds, *Solar Energy Materials and Solar Cells* 92 (2008) 1298–1301.
- [8] E. Bose, S. Karmakar, B.K. Chaudhuri, S. Pal, Importance of double-exchange interaction in low-doped ferromagnetic insulator  $\text{La}_{0.825}\text{Ca}_{0.125}\text{MnO}_3$ , *Solid State Communications* 145 (2008) 149–153.
- [9] X.D. Zhu, S.L. Li, X.J. Yang, J. Qiu, Microstructures and electrical properties of  $\text{La}_{0.8}\text{Sr}_{0.2}\text{MnO}_3$  films synthesized by sol–gel method, *Applied Surface Science* 254 (2007) 532–537.
- [10] Q. Li, L. Kuang, Y.M. Xuan, Prepared method and radiative properties of a thermochromic variable emittance material, *Journal of Engineering Thermophysics* 30 (2009) 1005–1008.
- [11] K. Shimazaki, A. Ohnishi, Y. Nagasaka, Computational design of solar reflection and far-infrared transmission films for a variable emittance device, *Applied Optics* 42 (2003) 1360–1366.
- [12] Y. Shimakawa, T. Yoshitake, Y. Kubo, T. Machida, K. Shinagawa, A. Okamoto, Y. Nakamura, A. Ochi, A variable-emittance radiator based on a metal-insulator transition of (La, Sr)MnO<sub>3</sub> thin films, *Applied Physics Letters* 80 (2002) 4864–4866.
- [13] S. Tachikawa, A. Ohnishi, Development of a variable emittance radiator based on a perovskite manganese oxide, *Journal of Thermophysics and Heat Transfer* 17 (2003) 264–268.
- [14] A. Ochi, T. Mori, Y. Shimakawa, Y. Kubo, A. Okamoto, Y. Nakamura, S. Tachikawa, A. Ohnishi, K. Shimazaki, Variable thermal emittance radiator using metal-insulator phase transition in  $\text{La}_{1-x}\text{Sr}_x\text{MnO}_3$ , *Japanese Journal of Applied Physics* 41 (2002) 7263–7265.
- [15] D.S. Fan, Q. Li, Y.M. Xuan, Emissivity and optical properties of thermochromic material  $\text{La}_{0.7}\text{Ca}_{0.3-x}\text{Sr}_x\text{MnO}_3$  ( $0 \leq x \leq 0.3$ ), *International Journal of Thermophysics* 32 (2011) 2127–2138.
- [16] K. Shimazaki, S. Tachikawa, A. Ohnishi, Y. Nagasaka, Radiative and optical properties of  $\text{La}_{1-x}\text{Sr}_x\text{MnO}_3$  ( $0 \leq x \leq 0.4$ ) in the vicinity of metal-insulator transition temperatures from 173 to 413 K, *International Journal of Thermophysics* 22 (2001) 1549–1561.
- [17] K.P. Shinde, S.S. Pawar, S.H. Pawar, Influence of annealing temperature on morphological and magnetic properties of  $\text{La}_{0.9}\text{Sr}_{0.1}\text{MnO}_3$ , *Applied Surface Science* 257 (2011) 9996–9999.
- [18] E.O. Chi, Y.N. Kim, J.C. Kim, N.H. Hur, A macroporous perovskite manganite from colloidal templates with a Curie temperature of 320 K, *Chemistry of Materials* 15 (2003) 1929–1931.
- [19] M.C. Wu, C.M. Chuang, Y.C. Huang, Y.J. Wu, K.C. Cheng, C.F. Lin, Y.F. Chen, W.F. Su, Nanopatterned optical and magnetic  $\text{La}_{0.7}\text{Ca}_{0.3}\text{MnO}_3$  arrays: synthesis, fabrication, and properties, *Proceedings of SPIE* 7603 (2010) 76031H.
- [20] J.H. Kim, A.M. Grishin, V.A. Ignatova, Wet etching study of  $\text{La}_{0.67}(\text{Sr}_{0.5}\text{Ca}_{0.5})_{0.33}\text{MnO}_3$  films on silicon substrates, *Journal of Electronic Materials* 37 (2008) 361–367.

- [21] S.B. Qin, D. Liu, H. Liu, Z.Y. Zuo, Size-dependent selective etching mechanism: cavity formation on barium titanate nanocubes, *Journal of Physical Chemistry C* 112 (2008) 17171–17174.
- [22] S.Q. Jiang, X.X. Ma, G.Z. Tang, Z.H. Wang, G. Wang, Z.H. Zhou, Microstructure and variable emittance property of annealed La–Sr–Mn–O films, *Journal of Rare Earths* 29 (2011) 83–86.
- [23] D.S. Fan, Q. Li, Y.M. Xuan, Investigation on radiative and optical properties of thermochromatic materials, *Journal of Engineering Thermophysics* 32 (2011) 1349–1352.
- [24] S. Maruyama, T. Kashiwa, H. Yugami, M. Esashi, Thermal radiation from two-dimensionally confined modes in microcavities, *Applied Physics Letters* 79 (2001) 1393–1395.
- [25] C.J. Fu, W.C. Tan, Semiconductor thin films combined with metallic grating for selective improvement of thermal radiative absorption/emission, *Journal of Heat Transfer* 131 (2009) 033105.
- [26] K.Q. Zhang, D.J. Li, *Electromagnetic Theory for Microwaves and Optoelectronics*, Second ed., Publishing House of Electronics Industry, Beijing, 2001.

www.spm.com.cn